To Be or Not to Be: Alicante-8, a Cluster or Not?

Randa Asa'd[1] , V. D. Ivanov[2] , I. Negueruela[3] , J. M John[1], A. Gonneau[4] , and M. Rejkuba[2]

[1] American University of Sharjah, Physics Department, P.O. Box 26666, Sharjah, UAE; raasad@aus.edu
[2] European Southern Observatory, Karl-Schwarzschild-Straße 2, D-85748 Garching bei München, Germany
[3] Departamento de Física Aplicada, Facultad de Ciencias, Universidad de Alicante, Carretera de San Vicente s/n, E-03690, San Vicente del Raspeig, Spain
[4] Institute of Astronomy, University of Cambridge, Madingley Road, Cambridge CB3 0HA, UK

Abstract

Recent surveys have uncovered new young massive clusters that host dozens of red supergiants (RSGs) near the inner Galaxy. However, many of them have still not been fully studied. Using Very Large Telescope/X-shooter near-infrared spectra, we present the first radial velocity analysis for the putative members of the candidate RSG cluster Alicante-8. Our results show a large dispersion of radial velocities among the candidate member stars, indicating that Alicante-8 does not seem to be a real cluster, unlike Alicante-7 and Alicante-10, which are confirmed by the distribution of the radial velocities of their RSG members. Measuring the spectral indices reveals that the assumption that the candidate stars are RSGs was incorrect, leading to the misclassification of Alicante-8 as a candidate RSG cluster. Our results imply that spectral classification based on the widely used CO band at 2.3 μm alone is not a sufficient criterion, because both red giants and RSGs can attain similar CO equivalent widths, and that spectroscopic radial velocities are needed in order to confirm unambiguously the cluster membership.

Unified Astronomy Thesaurus concepts: B supergiant stars (130); Young massive clusters (2049); Radial velocity (1332); Galactic center (565)

1. Introduction

The central regions of the Galaxy, in particular the area where the near side of the long Bar meets the spiral arms, has experienced recent rich star-forming activity, which created numerous young star clusters dominated by red supergiants (RSGs). Many of these young star clusters have been discovered in the past 12 years (Negueruela et al. 2010, 2011; González-Fernández & Negueruela 2012; Marco et al. 2014), but their detailed properties such as radial velocities, age, and metallicity have still not been fully studied. They all have high radial velocities ($v_{LSR} \approx +100\,km\,s^{-1}$), values that put them at distances close to 6 kpc from the Sun according to modern radial velocity rotation curves of the Milky Way (e.g., Davies et al. 2007).

In this work, we provide a comprehensive analysis of the candidate RSG members of the candidate cluster Alicante-8 (SIMBAD identifier: Cl Alicante 8) discovered by Negueruela et al. (2010), who found a concentration of bright red stars $\sim 16'$ away from the massive cluster RSGC1 (SIMBAD identifier: RSGC 1) They suggested that it was a cluster of RSGs in the region of the Scutum arm ($d \approx 6\,kpc$; Reid et al. 2019), containing at least eight RSGs that conformed to a very well-defined clump in different photometric diagrams, such as Q_{IR}/K_S, or $(J - K_S)/K_S$ where Q_{IR} is the infrared (IR) reddening-free color index. They assumed an age of 16–20 Myr for this candidate cluster, and a mass approaching 20,000 $M_\odot$ if the candidate RSG members can be confirmed. However, spectroscopic studies combined with radial velocity measurements are necessary to confirm the RSG nature of the stars and their membership in a cluster. Here, we address this issue with infrared spectroscopy to overcome the significant extinction to

this object. Negueruela et al. (2010) derived an average $E(J - K_S) = 2.7 \pm 0.2$ mag and $E(H - K_S) = 1.02 \pm 0.07$ mag, where the errors represent the dispersion in the individual values.

In this work, we carry out the first radial velocity analysis of the RSG candidates in this candidate cluster. Candidate members are hardly visible in the optical range due to the extinction toward the inner Galaxy, and so they need to be studied in the IR range. Only RSG candidates are readily identified; other members are too faint and cannot be distinguished in extremely crowded regions. The RSG candidates are present in Gaia EDR3 (Gaia Collaboration et al. 2021), but their astrometric parameters are very uncertain. Many have renormalized unit weight error (RUWE) > 1.4, indicating a poor astrometric solution, and in all cases the errors in the parallax are comparable to or larger than the parallax value itself.

The paper is organized as follows. In Section 2, we describe our data and data reduction. In Section 3 we obtain the radial velocities for our Alicante-8 candidate targets. We also confirm their accuracy by comparing our results to the literature radial velocities for RSGs in Alicante-7 (SIMBAD identifier: Cl Alicante 7) and Alicante-10 (SIMBAD identifier: Cl Alicante 10). Those results are presented in Section 4. In Section 5 we provide new detailed spectral diagnostics for our sample using two independent methods. After that we discuss Gaia EDR3 proper motions in Section 6 and summarize our findings in Section 7.

2. Data and Data Reduction

We analyzed the near-infrared (NIR) spectra for a sample observed with Very Large Telescope (VLT)/X-shooter (D'Odorico et al. 2006; Vernet et al. 2011) in service mode under ESO program number 0103.D-0881(A) (PI R. Asad). The sample was selected based on the RSG candidates of Alicante-8 (Negueruela et al. 2010), with the finding chart
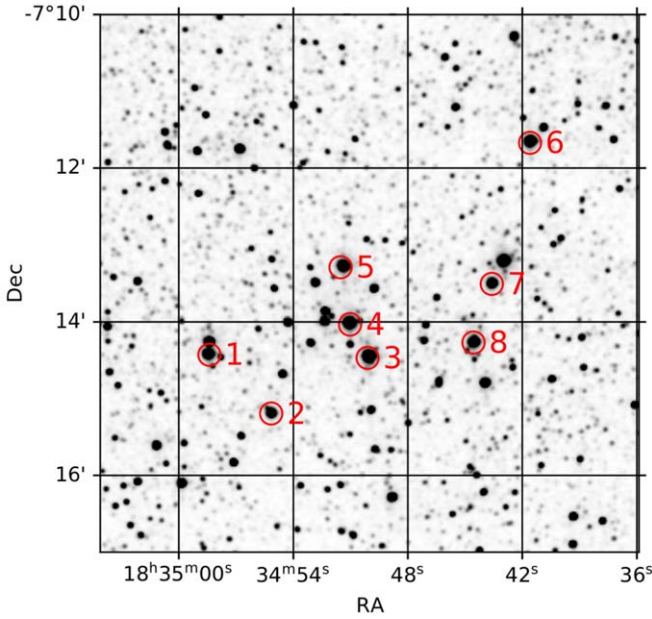
Figure 1. Two Micron All Sky Survey (2MASS) K_S-band finding chart for the Alicante-8 candidate member stars from Negueruela et al. (2010). It is a linearly scaled 2MASS K_S-band image with a field of view of $\sim 7' \times 7'$, centered at (R.A., decl.) $\sim$ (18:34:50, -07:13:30). North is up and east is left.

Table 1
Positions and Radial Velocities in km s^{-1} of the Target Stars

| Cluster/Star	R.A. (J2000)	Decl. (J2000)	RV[a]	RV[b]	S/N
Alicante-7					
S14	18:44:27.00	-03:29:42.00	85 ± 0.6	84	216
S43	18:44:29.57	-03:30:04.68	75 ± 0.5	79	178
S55	18:44:39.64	-03:29:59.60	108 ± 0.6	107	163
S64	18:44:46.96	-03:31:09.70	63 ± 0.5	63	189
S76	18:44:20.68	-03:28:45.52	74 ± 0.5	75	171
S96	18:44:30.40	-03:28:49.22	71 ± 0.6	73	160
Alicante-10					
S67	18:45:11.25	-03:39:36.14	71 ± 0.6	74	191
S90	18:45:36.53	-03:39:21.92	16 ± 0.5	17	173
S91	18:45:17.13	-03:41:25.91	75 ± 0.5	75	178
Alicante-8					
S1	18:34:58.40	-07:14:27.46	-33 ± 0.5		174
S2	18:34:55.28	-07:15:11.59	71 ± 0.6		92
S3	18:34:50.23	-07:14:28.07	37 ± 0.5		146
S4	18:34:51.15	-07:14:02.11	88 ± 0.7		43
S5	18:34:51.65	-07:13:17.65	-9 ± 0.5		102
S6	18:34:41.72	-07:11:40.34	111 ± 0.6		112
S7	18:34:43.72	-07:13:30.61	-4 ± 0.6		110

Notes. The signal-to-noise ratios (S/Ns) of the spectra are also listed.
[a] Radial velocities obtained in this work using Equation (1).
[b] Radial velocities from the literature.

shown in Figure 1. Stars 1–7 of Negueruela et al. (2010) were observed, but their Star 8 was not.

In addition to the candidates of Alicante-8, our observed sample consists of RSGs in Alicante-7 and Alicante-10 selected from Negueruela et al. (2011) and González-Fernández & Negueruela (2012) respectively, for which radial velocities were derived by Origlia et al. (2019), in order to test our method.
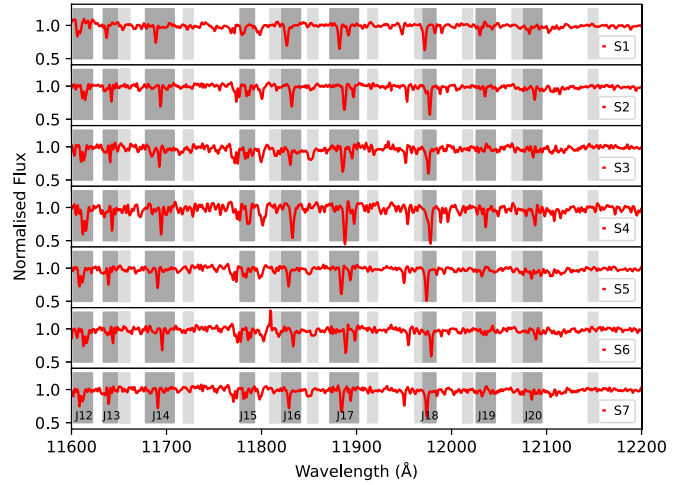
Figure 2. VLT/X-shooter J-band spectra of the targets analyzed in this work. Numbers as in Negueruela et al. (2010).

Our observations provide continuous spectral coverage over $0.3-2.4$ μm. With 2×30 s integration time in the NIR, we were able to obtain typical signal-to-noise ratio (S/N) > 100. At shorter wavelengths, the spectra would not be useful given the very high extinction, and therefore only the NIR data were used. Details about the S/N of each RSG are listed in Table 1. The average S/N for our sample is 111. We used the $0.''9$ slit for the NIR channel. This gives a resolution higher than $R \sim 5600$. We used the advanced data products for our observed sample from the ESO archive. The spectra were processed by applying the standard spectroscopic data reduction steps[5] as described in the associated data release description available on the ESO Phase 3 website[6] (version 3.3.0). We corrected the 1D-extracted and flux-calibrated spectra for telluric absorption using molecfit (Kausch et al. 2015; Smette et al. 2015), following the same approach developed for the X-shooter Spectral Library (Gonneau et al. 2020). We first applied molecfit to the entire near-IR spectrum to derive the precipitable water vapor column (PWV), then divided the spectrum into smaller wavelength segments and applied molecfit locally using the PWV value determined before. The corrected wavelength segments were then merged together. The continuum-normalized spectra are presented in Figures 2–4. The normalization was performed using IRAF[7] (Tody 1986, 1993).

3. Method

We obtained the radial velocity using our updated full-spectrum fitting program (see Asa'd et al. 2013, 2016; Asa'd 2014), which applies a χ^2 minimization to compare our observed spectra with a model spectrum created by using model atmospheres based on local thermal equilibrium spherical 1D RSG-MARCS models (Gustafsson et al. 2008), with the default technical parameters for line synthesis on the web server.[8] The model spectrum represents a synthetic star with an effective temperature $= 4400.0$ K, log $g = 0.00$, metallicity $= 0.00$, and microturbulence velocity $= 3.00$. The
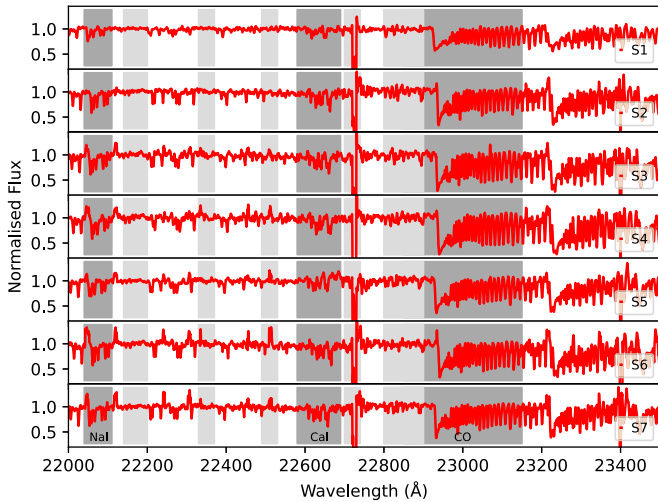
Figure 3. VLT/X-shooter *K*-band spectra of the targets analyzed in this work. Numbers as in Negueruela et al. (2010).

Figure 4. VLT/X-shooter *H*-band spectra of the targets analyzed in this work. Numbers as in Negueruela et al. (2010).

spectrum covers the wavelength range 11600–12200 Å and has a resolution of $R = 20,000$ (see Asa'd et al. 2020, for more details).

We calculate the heliocentric radial velocity for our sample according to the equation[9]

$$RV = rv + HC + (rv \times HC/c). \qquad (1)$$

Here rv is the radial velocity obtained from the cross-correlation with the synthetic spectrum, HC is the heliocentric correction calculated using the coordinates of each observed star and utilizing the `jplehem` package in Python (Rhodes 2011), and *c* is the speed of light.

To confirm the accuracy of our method, we first apply it to our observed sample of RSGs in Alicante-7 and Alicante-10 that have radial velocities estimated in Origlia et al. (2019). The upper part of Table 1 shows an excellent agreement between our velocities and those in the literature for most objects within each cluster.

Note that in Table 1 the IDs used for Alicante-7 and Alicante-10 stars reflect the unique OB numbers given during the observing run; however, the IDs used for Alicante-8 stars follow the numbering system of Negueruela et al. (2010) for easier comparison with their work.

We obtained the precision of the estimated radial velocity as a function of input radial velocity and S/N, by creating 120,060 mock RSGs (generated at random points within the parameter space of the original model grid) and shifting the spectra to radial velocities from -120 to $110 \, \mathrm{km \, s^{-1}}$ in steps of $10 \, \mathrm{km \, s^{-1}}$, then adding 200 different realizations of random Gaussian noise ranging from $S/N = 40$ to $S/N = 300$ in steps of 10. We then aimed to recover the original input radial velocities for this sample using our fitting program. The errors listed in Table 1 represent the standard deviation of the mock sample per radial velocity and S/N. This method has been used previously in Asa'd & Goudfrooij (2020), Goudfrooij & Asa'd (2021), and Asa'd et al. (2021).

4. Radial Velocities

The lower part of Table 1 shows the radial velocity estimates for the candidates in Alicante-8. The derived heliocentric radial
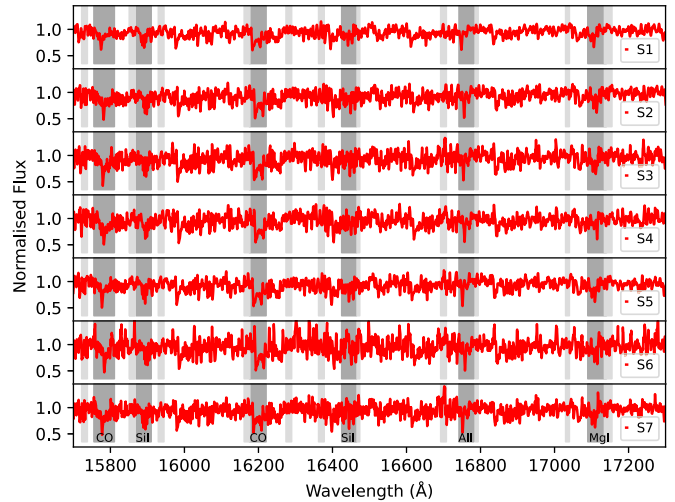
velocities span a wide range of values (from -33 to $+111$ $\mathrm{km \, s^{-1}}$). Given the large dispersion of radial velocities among the member candidates, Alicante-8 does not seem to be a real cluster, unlike other similar candidates, such as Alicante-7 and Alicante-10, which are confirmed by the distribution of RVs (see here and Origlia et al. 2019). In fact, given that the correction from heliocentric to LSR in this direction is approximately $+15 \, \mathrm{km \, s^{-1}}$, the radial velocities of stars 1, 5, and 7 are negative, which is completely incompatible with the expectation for an RSG at a distance of 6 kpc, which is $\sim +75 \pm 10 \, \mathrm{km \, s^{-1}}$ (see Table 1 for the values of Alicante-7 and Alicante-10, which are in the same region). It is worth considering the reasons that lead to this misidentification.

Lacking confirmatory RV data, Negueruela et al. (2010) estimated the possibility that Alicante-8 represented a random overdensity of field stars, concluding that a random grouping of RSGs was extremely unlikely. The weak point in their reasoning was the assumption that all the stars were indeed RSGs. In fact, considering the weakness of the metallic features in the spectra presented in Figures 2–4, most of the putative members are unlikely to be RSGs, but rather less luminous red giants. Only S4, which Negueruela et al. (2010) identified as the most luminous candidate member, has a spectrum similar to the RSGs in nearby clusters and a radial velocity compatible with an RSG in the Scutum complex.

5. Spectral Diagnostics

In this section, we evaluate the assumption that the candidate stars of Alicante-8 are RSGs by using two independent methods.

5.1. Using EW of Spectral Indices

Messineo et al. (2021) defined a number of spectral indices sensitive to stellar temperature and surface gravity that can separate between giants and supergiants based on their equivalent width. To apply these same diagnostic tools directly, we convolved our spectra for Alicante-8 candidates with a Gaussian to match the moderate resolution of SpeX data ($R = 2000$) in Messineo et al. (2021). The IRAF task sband was then used for measuring these spectral indices.
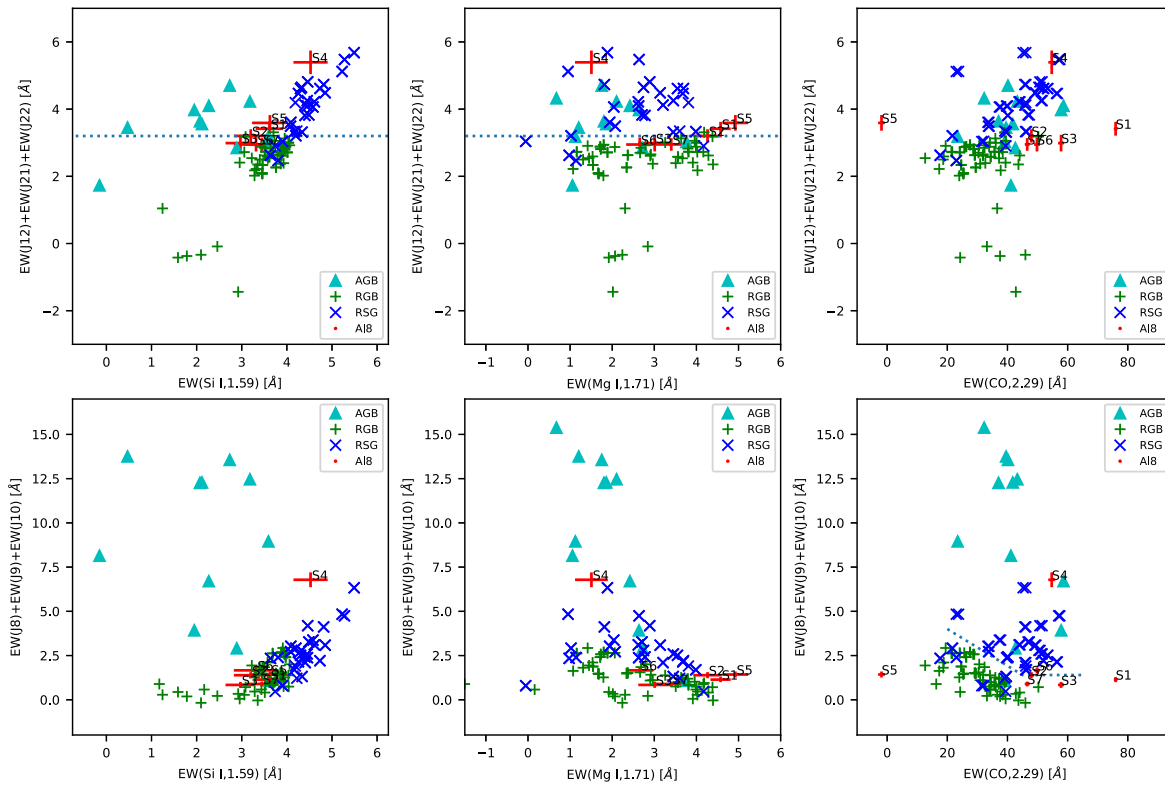
Figure 5. Luminosity classification of the targets in the field of Alicante-8 (red dots). RSGs, RGB stars, and asymptotic giant branch (AGB) stars from the sample of Rayner et al. (2009) are shown. The dotted lines indicate the borders of the RSG loci, defined by Messineo et al. (2021). The spectral indices used on the axes are shown in Figures 2–4. See text for more details.

The resulting spectral indices for our sample stars are compared with the spectral indices of RSGs, red giants, and asymptotic giant branch stars from the sample of Rayner et al. (2009) in their Figure 3. The spectral indices used on the x and y axes are marked in Figures 2–4. For detailed definitions of the spectral indices, see Messineo et al. (2021). Figure 5 shows that the majority of our targets fall in the transition region between RSGs and red giant branch (RGB) stars, with only S4 falling clearly inside the RSG locus, implying that Alicante-8 is not a young massive cluster.

We obtained the errors shown in the figure by generating 100 artificial spectra for each of the 13 spectra by Monte Carlo bootstrapping, then remeasured the spectral indices and calculated the rms of the measurements. We stress that the errors are conservative, because we measured the rms locally within a sliding window (41 pixels wide), so this includes extra contribution from sharp telluric absorption lines and spectral slope. Nevertheless, the errors are small.

5.2. Using K-band Spectra

Negueruela et al. (2010) lacked the J-band part of the NIR spectra, and they relied on K-band spectra only to classify the stars. In this spectral range (2.1 μm < λ < 2.4 μm) spectral lines, other than Na and Ca, are relatively weak and the main spectral features are strong CO bandheads that are detected as absorption features in late-type stars. The strength of these CO bandheads—measured as the equivalent width (EW) of the first band—correlates with decreasing temperature (i.e., later spectral type) and with increasing luminosity. Spectral types were estimated by means of these correlations by referring to a calibration worked out by Davies et al. (2007), which was re-

evaluated by Negueruela et al. (2010) by adding a large number of measurements from spectra in the atlas of Rayner et al. (2009). The calibration is degenerate, in the sense that both red giants and RSGs can attain similar values of the EW. A red giant will have a much lower value than an RSG of the same spectral type, but a red giant of a later spectral type may have a value comparable to an RSG of an earlier type. Based on the calibration, Negueruela et al. (2010) concluded that any star with EW > 24 Å (for the spectral ranges defined in their paper) is almost certainly a supergiant, while any star with EW $\gtrsim$ 22 Å is very likely a supergiant. While the separation is moderately well-defined for M-type stars, K-type supergiants are problematic, because they typically have EW ≈ 20–22 Å.

The measurements of Negueruela et al. (2010) showed that most stars were close to the lower limit for an RSG, leading to a classification as K supergiants for stars 1, 2, 5, and 7. With the information obtained here, it is clear that these stars are not K supergiants but M giants—both can have the same EW. For confirmation, we have measured again the EW of the first CO bandhead at 2.2935 μm in the same way as done by Negueruela et al. (2010), i.e., by selecting the same continuum and integration regions. Our measurements have been done on both the X-shooter spectra and their original William Herschel Telescope (WHT) spectra. The latter have lower resolution, $R \sim 2500$. We find differences of typically 2 Å between the EWs measured on the WHT and X-shooter spectra, but they do not appear to be systematic.[10] Although some degree of spectral variation cannot be ruled out, we suspect that continuum normalization can have a strong impact on the

---

[10] Based on the seven stars in common.

Table 2
Gaia EDR3 Data for Candidate Members of Alicante-8 from Negueruela et al. (2010), Together with Photogeometric Distances from Bailer-Jones et al. (2021)

| Star	ϖ (mas)	d (kpc)	pmRA (mas a^{-1})	pmDE (mas a^{-1})	RUWE	G
S1	-0.3297 ± 0.2308	$6.3^{+2.4}_{-2.1}$	-0.662 ± 0.269	-1.986 ± 0.229	1.68	17.71 ± 0.04
S2	-0.2942 ± 0.3064	$6.4^{+2.4}_{-2.1}$	-1.854 ± 0.351	-2.695 ± 0.300	1.20	18.85 ± 0.01
S3	-0.0902 ± 0.2434	$5.7^{+2.1}_{-2.1}$	-0.964 ± 0.277	-5.726 ± 0.232	2.04	17.68 ± 0.01
S4	0.6222 ± 0.717	$6.9^{+1.1}_{-1.0}$	-1.032 ± 0.815	-5.108 ± 0.706	1.40	20.05 ± 0.02
S5	0.2502 ± 0.275	$4.8^{+2.4}_{-1.6}$	-3.276 ± 0.297	-7.537 ± 0.253	1.52	18.46 ± 0.01
S6	-0.0051 ± 0.3928	$5.7^{+2.9}_{-1.8}$	-2.127 ± 0.462	-6.021 ± 0.398	1.29	19.09 ± 0.02
S7	0.5966 ± 0.2733	$3.7^{+1.9}_{-1.1}$	-3.831 ± 0.288	-6.55 ± 0.246	1.40	18.52 ± 0.01
S8	0.5265 ± 0.2293	$3.3^{+1.9}_{-1.2}$	-0.676 ± 0.263	-2.859 ± 0.23	1.21	18.02 ± 0.04

measurement of the EWs, leading to a systematic error in the measurement of ± 2 Å, which dominates the uncertainty budget

All the stars have EWs between 18 and 21 Å, just below the separation line. As they occupy similar locations in all the diagnostic diagrams shown in Figure 5, we conclude that they are either very luminous or very late giants. We speculate that small systematic or random effects in the measurements of Negueruela et al. (2010) may have pushed the EWs for some stars upwards by 1–2 Å, moving them into the region of M-type RSGs. Those with lower EW measurements were then assumed to be K supergiants. Again, the exception is S4, which (with EW = 25 ± 2 Å) definitely falls in the same region as the supergiants, similar to most diagrams in Figure 5.

6. Proper Motions

We have downloaded Gaia EDR3 (Gaia Collaboration et al. 2021) data for all the putative cluster member stars. They are listed in Table 2. The results are poor in all cases, and no reliable information can be obtained about the distances to the sources. The proper motions, although affected by large errors, show such a large dispersion that the stars cannot belong to a single population. Only S3 and S4 have compatible proper motions (but the errors for the latter are huge (± 0.717)). In Figure 6 we compare the proper motions of stars S1–S8 with the proper motions of all stars in a circle of radius 3′. To make the comparison more meaningful, we plotted the color–magnitude diagram (CMD) of all the stars brighter than $G = 20$ (fainter objects had very large errors in all astrometric measurements and were not used) having plx < 0.5 mas (i.e., $d > 2$ kpc). The CMD shows an apparent "main sequence" corresponding to the field population (in all likelihood, mainly stars at distances comparable to the Scutum–Crux arm; see Marco & Negueruela 2011 for a discussion of Galactic structure in this direction and Negueruela et al. 2010 for the run of extinction along this sightline). Objects with colors redder than this sequence are marked as blue dots in Figure 6, as they are mostly the sort of distant, either intrinsically red or obscured (or both) objects with which our candidates must be compared. The candidate RSGs are spread over a significant part of the space occupied by field stars, with two objects (S5 and S7) displaying higher proper motion values than most other stars. This all again suggests that the stars are mostly unrelated.

Based on their photometric behavior, Gaia Collaboration et al. (2021) classifies stars S1, S3, S5, S7, and S8 as long-period variables. However, parameters are derived for only two stars: (I) S1 has an amplitude of variability of 0.69 mag and a period of 322.6 days, and (II) S8 has an amplitude of 0.81 mag
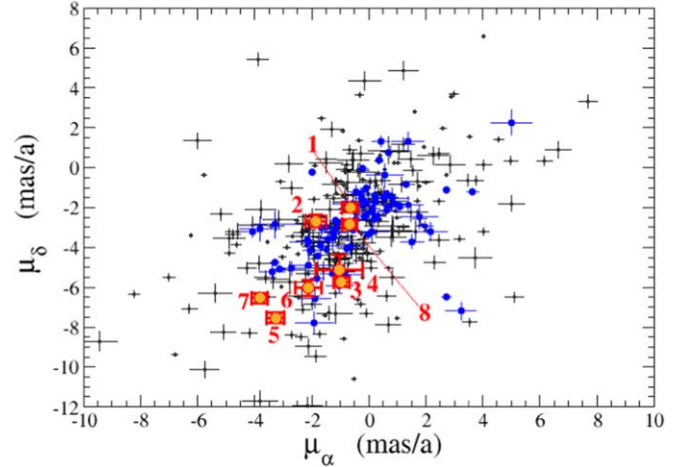
Figure 6. Proper motions of stars in a 3′ circle around the nominal center of Alicante-8. Stars S1–S8 are marked as large orange circles. The blue circles represent objects with redder than typical colors (see text for details), i.e., the population to which the candidate members must be compared. We note that they are more tightly concentrated than the general population, but our objects are clearly divergent.

and a period of 384.6 days. These values are compatible with luminous AGB stars (Whitelock et al. 2008).

In Table 2, we include the photogeometric distances from Bailer-Jones et al. (2021). These are estimated with a prior that includes a model of the distribution of stellar magnitudes in a given direction and utilizes the color and magnitude of the stars. Although individual Gaia measurements of distance to the candidate member stars carry significant uncertainties, the bulk of them are entirely consistent with a distance ~6 kpc, where clusters of RSGs are located. Nevertheless, stars S7 and S8 seem to be clearly in the foreground of the Scutum arm.

7. Summary and Conclusion

Using VLT/X-shooter NIR spectra (11600−12200 Å) of nine RSGs in Alicante-7 and Alicante-10 and seven candidate stars in Alicante-8, we performed a detailed spectroscopic analysis that we summarize below.

(A) We confirm the radial velocity of the RSGs in Alicante-7 and Alicante-10. Our measurements are in excellent agreement with those of Origlia et al. (2019).

(B) We present the first radial velocity estimates for the candidate member stars of the putative cluster Alicante-8. Our results show a large dispersion in radial velocity, indicating that Alicante-8 is likely not a bound cluster.

(C) We stress that spectra (not photometry) with sufficiently high resolving power to measure radial velocities are necessary to confirm cluster membership. The resolution of VLT/X-shooter provides accurate radial velocities.

(D) We estimated the luminosity class of the stars based on spectral indices sensitive to the surface gravity in Messineo et al. (2021, their Figures 4 and 5) to evaluate the assumption that the bright potential members of Alicante-8 are RSGs. Most objects fall in between the RGB and AGB loci, rather than in the RSG locus, suggesting that these stars are not RSGs.

(E) We conclude that using the K-band part of the NIR spectra alone does not provide reliable means to classify stars, due to the degeneracy between 2.3 μm CO EWs with different spectral types—both giants and RSGs can attain similar values of the EWs. This is an important caveat to keep in mind for studies of stars in young massive clusters as well as field stars near the inner Galaxy.

The spectral data used in this work are available from the ESO Science Archive under program ID 0103.–0881(A). The telluric-absorption-corrected and continuum-normalized spectra are available upon request.

ORCID iDs

Randa Asa'd ⓘ https://orcid.org/0000-0003-4861-6624
V. D. Ivanov ⓘ https://orcid.org/0000-0002-5963-1283
I. Negueruela ⓘ https://orcid.org/0000-0003-1952-3680
A. Gonneau ⓘ https://orcid.org/0000-0001-9091-5666
M. Rejkuba ⓘ https://orcid.org/0000-0002-6577-2787

References

Asa'd, R., & Goudfrooij, P. 2020, MNRAS, 498, 2814
Asa'd, R., Goudfrooij, P., As'ad, A. M., et al. 2021, MNRAS, 505, 979
Asa'd, R., Kovalev, M., Davies, B., et al. 2020, ApJ, 900, 138
Asa'd, R. S. 2014, MNRAS, 445, 1679
Asa'd, R. S., Hanson, M. M., & Ahumada, A. V. 2013, PASP, 125, 1304
Asa'd, R. S., Vazdekis, A., & Zeinelabdin, S. 2016, MNRAS, 457, 2151
Bailer-Jones, C. A. L., Rybizki, J., Fouesneau, M., Demleitner, M., & Andrae, R. 2021, AJ, 161, 147
Davies, B., Figer, D. F., Kudritzki, R.-P., et al. 2007, ApJ, 671, 781
D'Odorico, S., Dekker, H., Mazzoleni, R., et al. 2006, Proc. SPIE, 6269, 626933
Gaia Collaboration, Brown, A. G. A., Vallenari, A., et al. 2021, A&A, 649, A1
Gonneau, A., Lyubenova, M., Lançon, A., et al. 2020, A&A, 634, A133
González-Fernández, C., & Negueruela, I. 2012, A&A, 539, A100
Goudfrooij, P., & Asa'd, R. S. 2021, MNRAS, 501, 440
Gustafsson, B., Edvardsson, B., Eriksson, K., et al. 2008, A&A, 486, 951
Kausch, W., Noll, S., Smette, A., et al. 2015, A&A, 576, A78
Marco, A., & Negueruela, I. 2011, A&A, 534, A114
Marco, A., Negueruela, I., González-Fernández, C., et al. 2014, A&A, 567, A73
Messineo, M., Figer, D. F., Kudritzki, R.-P., et al. 2021, AJ, 162, 187
Negueruela, I., González-Fernández, C., Marco, A., & Clark, J. S. 2011, A&A, 528, A59
Negueruela, I., González-Fernández, C., Marco, A., Clark, J. S., & Martínez-Núñez, S. 2010, A&A, 513, A74
Origlia, L., Dalessandro, E., Sanna, N., et al. 2019, A&A, 629, A117
Rayner, J. T., Cushing, M. C., & Vacca, W. D. 2009, ApJS, 185, 289
Reid, M. J., Menten, K. M., Brunthaler, A., et al. 2019, ApJ, 885, 131
Rhodes, B. C. 2011, PyEphem: Astronomical Ephemeris for Python, Astrophysics Source Code Library, ascl:1112.014
Smette, A., Sana, H., Noll, S., et al. 2015, A&A, 576, A77
Tody, D. 1986, Proc. SPIE, 627, 733
Tody, D. 1993, in ASP Conf. Ser. 52, Astronomical Data Analysis Software and Systems II, ed. R. J. Hanisch, R. J. V. Brissenden, & J. Barnes (San Francisco, CA: ASP), 173
Vernet, J., Dekker, H., D'Odorico, S., et al. 2011, A&A, 536, A105
Whitelock, P. A., Feast, M. W., & Van Leeuwen, F. 2008, MNRAS, 386, 313